International Journal of Latest Engineering and Management Research (IJLEMR)
ISSN: 2455-4847
www.ijlemr.com || Volume 09 – Issue 03 || March 2024 || PP. 64-70

Active Uniform Field Design of 7T Liquid Helium-Free Magnetic Resonance Superconducting Magnets

MingYan[1,2], Heyang Wang[1,2*], and Pengfei Wu[1,2]
[1]*University of Chinese Academy of Sciences, Beijing 100094, China*
[2]*Institute of Electrical Engineering, Chinese Academy of Sciences, Beijing 100190, China*
[*]*Corresponding author*

Abstract: The uniformity of the magnetic field in a 7T liquid-helium-free magnetic resonance superconducting magnet is achieved through a comprehensive design approach. This involves conducting harmonic analysis to decompose the main harmonics and employing active uniform field design to counteract harmonics of each order. Initially, the distribution characteristics of the strong magnetic field generated by the magnet are analyzed, and a two-dimensional magnetic field distribution map of the 8th order harmonics is obtained through harmonic analysis in the target region. Subsequently, the structure of the radial homogenizing coil is optimized, and the homogenizing environment is simulated and analyzed. The results demonstrate that the homogenizing optimization leads to a peak homogeneity of 80.45 ppm in a spherical imaging space with a radius of 15 mm. Moreover, the magnetic field in the target area is reduced from 107.41 ppm to 80.45 ppm, thereby enhancing the uniformity of the magnetic field in the target space.

Keywords: Liquid helium-free magnetic resonance superconducting magnets; Uniform field coils; Harmonic analysis; Quantum genetic optimization

Introduction

Magnetic Resonance Imaging (MRI) is a significant advancement in medical imaging, following computerized scanning technology. To enhance the strength and reliability of the magnetic field at the center, superconducting magnets without current loss are commonly utilized. These magnets enable higher signal-to-noise ratios and resolution, revealing more detailed information compared to low-field MRI. Additionally, they facilitate imaging at the molecular level, which is particularly advantageous for studying the functional and metabolic aspects of tissues. This molecular-level imaging is especially valuable in the field of brain cognitive science [1-3].

During experiments with MRI, the presence of inhomogeneous magnetic fields can result in distorted and misaligned reconstructed images, making them difficult to differentiate. Therefore, to ensure high-quality magnetic resonance results, it is crucial for magnetic resonance instruments to have magnets with a high degree of magnetic field uniformity. The uniformity of the magnetic field is a significant factor that impacts the quality of the imaging. However, the processing and assembly of the magnet can cause deviations from the ideal design value in terms of magnetic field uniformity. Additionally, small sources of interference, such as electronic components loaded on the probe inserted into the magnet and thermocouple components of the temperature control system placed around the magnet, can also affect the uniformity of the magnetic field. Therefore, achieving uniformity in the magnetic field is a critical step for the success of the test. Homogenization techniques can be broadly categorized into two types: active homogenization and passive homogenization [4-6]. Active homogenization involves using the magnetic field generated by the homogenizing coil, which is energized with electric current, to offset the inhomogeneous component of the main magnetic field. This method is currently considered more effective and widely applicable [8]. Traditional computational methods typically employ numerical techniques such as the analytical method, boundary element method, target field method, and spherical function. However, these methods often encounter challenges related to a large number of iterations and computational complexity. With the rapid advancement of artificial intelligence, new bionic optimization algorithms are being widely adopted due to their speed and intelligence.

This paper utilizes the initial measured field data from a 7T liquid-free helium magnetic resonance superconducting magnet to optimize the design of magnetic field uniformity in the target region. It achieves this by establishing an active uniform field analytical solution model and a quantum genetic algorithm optimization model. These models offset the inhomogeneous component of the main magnetic field using the magnetic field generated by the uniform field coils when energized by electric current. The correctness of the methodology proposed in this paper is verified through a simulation model.

Harmonic analysis of the target magnetic field

Harmonic analysis

The initial magnetic field data is visualized on a spherical surface, as depicted in Figure 1. In the spherical coordinate system, the magnetic field on the sphere is decomposed into a series of harmonic sums. These harmonic sums are then converted to the right-angle coordinate system [9], as shown in equation (1).

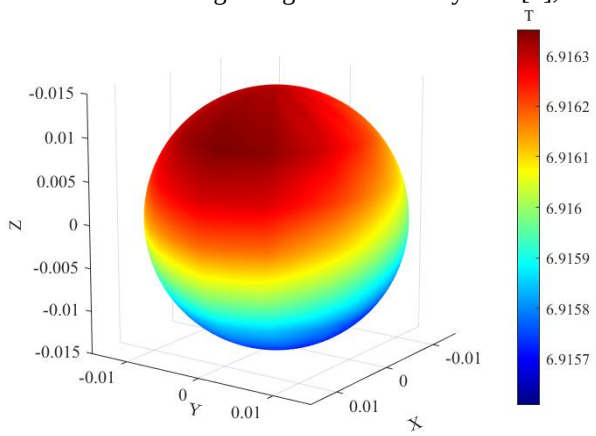

Fig. 1 Visualization of Uniform Magnetic Field

The homogenizing coils are designed to offset first-order harmonics. Typically, active homogenizing methods are effective in offsetting low-order harmonics, while passive homogenizing methods are employed to offset higher-order harmonics. This paper focuses on analyzing harmonics from the first to the eighth order, and the obtained harmonic coefficients are presented in Table 1.

Table 1 Magnetic field strengths of iron bars with uniform field of each order and corresponding magnetic field values at the target point

Uniform field coil	Ordinal number*n*	Number of degrees *m*	Dissociation A_n^m	Target magnetic field
Z1	1	0	0.025	A_1^0Zt
X	1	1	0.010	A_1^1Xt
Y	1	-1	-0.002	B_1^1Yt
Z2	2	0	-0.371	$A_2^0[2Zt^2-(Xt^2+Yt^2)]$
ZX	2	1	-0.022	$A_2^1 \cdot Zt \cdot Yt$
ZY	2	-1	-0.078	$B_2^1 \cdot Zt \cdot$ Yt
X2-Y2	2	2	0.010	$A_2^2 \cdot(Xt^2-Yt^2)$
XY	2	-2	0.130	$B_2^2 \cdot Xt \cdot Yt$

Fig. 2 shows the 2D magnetic field distribution of the 8th order harmonics.

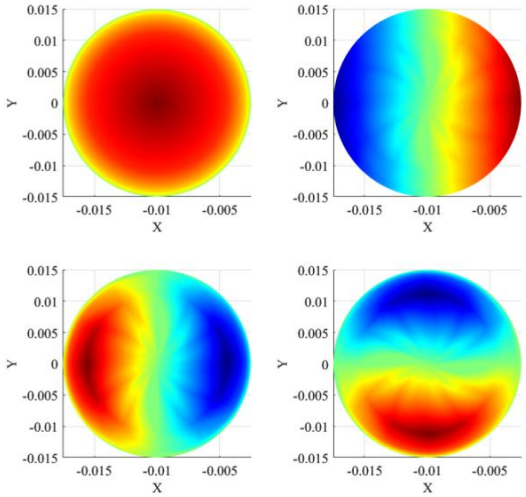

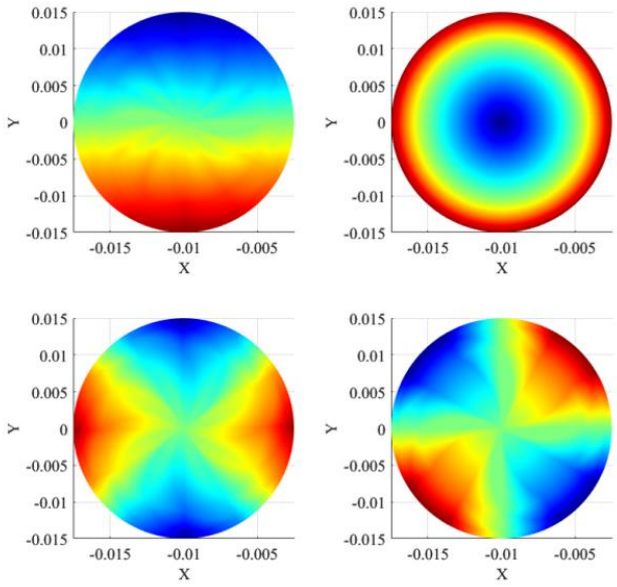

Fig. 2. 2D magnetic field distribution for the first 8 order harmonics

$$B_z = A_0 + A_1^0 z + A_1^1 x + B_1^1 y + A_2^0[z^2 - \frac{(x^2+y^2)}{2}] + 3A_2^1 zx + 3B_2^1 zy + 3A_2^2(x^2-y^2) + 6B_2^2 xy$$
$$+A_3^0 z[z^2 - \frac{3(x^2+y^2)}{2}] + 6A_3^1 x[6z^2 - \frac{3(x^2+y^2)}{2}] + 6B_3^1 y[6z^2 - \frac{3(x^2+y^2)}{2}] \quad (1)$$
$$+15A_3^2 z(x^2-y^2) + 30B_3^2 xyz + 15A_3^3 x(x^2-3y^2) + 15B_3^3 y(3x^2-y^2)$$

Where the A, B are the defined target magnetic fields and x, y, z are the coordinates of the target region.

Active Uniform Field Coil Design Principles

The magnetic field in the imaging region of a magnetic resonance imaging system can be decomposed into harmonic components, each corresponding to a set of homogenizing coils. There are two main types of active homogenizing coils: solenoidal coils, which cancel out the axial harmonic components of the magnetic field, and saddle coils, which cancel out the radial harmonic components. These coils are also referred to as axial homogenizing coils and radial homogenizing coils, respectively. When using the analytical method for computation, the coil space width and radial dimensions are ignored, and the coil is treated as an ideal single conductor. Figure 3 illustrates the results of the axial uniform field coil and the radial uniform field coil, both designed using the analytical method. In this case, the radial uniform field coil shown in Figure 3 is a saddle coil.

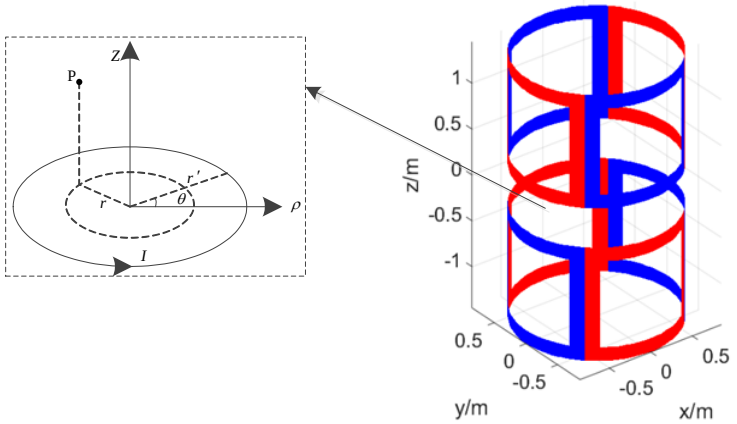

Fig. 3 Structure of Radial Uniform Field Coil

For axial uniform field coils Z1 and Z2, as in Fig. 3 two pairs of current loops are arranged symmetrically on each side of the z = 0 plane, where coil Z1 is arranged antisymmetrically and coil Z2 positively symmetrically, and any point on the coils is connected to the origin of the coordinates, and the angle of the line with the z-axis is defined as the α-angle. By many circular coils of the same radius, each of which can be set to a different number of turns, it is known through the theorem of magnetic field superposition that the magnetic field generated by multiple coils can be superimposed to obtain the final target magnetic field [10-15].

If the arc current is *I*, the radius is *a*, and the corresponding central angles of the circle at the two ends are θ_1, θ_2. The axial magnetic induction B_Z produced at point *P* in space is

$$B_Z = \frac{\mu_0 Ia}{4\pi}\int_{\theta_1}^{\theta_2}\frac{a - x\cos\alpha - y\sin\alpha}{r^3}d\alpha \tag{2}$$

$$r = \sqrt{a^2 + x^2 + y^2 + (z - z_0)^2 - 2a\left(x\cos\alpha + y\cos\alpha\right)} \tag{3}$$

Where the μ_0 is the vacuum permeability, *I* is the current, and *a* is the radius. For Y and ZY uniform field coils, they are obtained by rotating the X and ZX coils by 90° around the Z axis; the XY uniform field coil is obtained by rotating the X2-Y2 uniform field coil by 45°. The magnetic induction in the z-axis direction at point P can be written as

$$B_Z = \frac{\mu_0 I \cdot \left[F\left(K(k), Z, r, \rho, E(k)\right)\right]}{2\pi\sqrt{Z^2 + (r+p)^2}} \tag{4}$$

In (4), the current *I*is a variable and $F\left(K(k), Z, r, \rho, E(k)\right)$ is a constant quantity, the detailed formula is

$$F = K(k) - \frac{Z^2 - r^2 + \rho^2}{Z^2 + (r-\rho)^2}E(k) \tag{5}$$

In (5), *r* is the radius, *Z* and are the coordinates, and is the magnetic permeability. For an *N*-turn coil, the Z-axis magnetic induction at a point P is

$$B_{ZN} = \frac{\mu_0\left[F\left(K(k), Z, r, \rho, E(k)\right)\right]}{2\pi\sqrt{Z^2 + (r+\rho)^2}} \cdot I \cdot N \tag{6}$$

The variables in (6) are the current *I* and the number of turns *N*. These two variables are used as two "populations", which are searched in the space of the two variables by bit coding, quantum rotation, ground state crossing and bit decoding to find the combined value of the magnetic induction that makes the magnetic induction at the point P reach the target magnetic induction [16-22].

Active homogenizing field design options and results

Based on the design method of active uniform field in the previous section, calculate the optimization calculation of 8 groups of uniform field coils. Based on the above analysis of the 8 sets of magnetic field harmonics, the mathematical model for constructing the coil design is

$$\begin{aligned} &Minimize: \sum_{i=1}^{8} V_i \\ &Subject\ \ to: \begin{cases} I_i \le 3A \\ 0 \le \theta_{1,2} \le 90° \\ 0 \le \theta_{3,4} \le 45° \\ 0 \le \theta_{5,6} \le 45° \\ 10° \le \alpha_{1,2,3,4} \le 90° \end{cases} \end{aligned} \tag{10}$$

Where V_i is the difference between the magnetic field generated by the uniform field coil and the target magnetic field value, I_i is the current passed through the X, Y, ZX, ZY, X2-Y2, and XY coils, respectively, θ_i is the angle corresponding to the six sets of coils, respectively, and α_i is the elevation angle corresponding to the Z1 and Z2 coils, respectively.

Table 3 Parameters of uniform field coils

Transformers	X	XZ	X2-Y2	Z1		Z2	
Current(A)	1.44	2.35	1.65	0.48		0.99	
Angle (°)	68.00	43.00	23.00	20.87	35.01	12.74	26.03

The quantum genetic algorithm and Bayesian optimization algorithm were utilized to solve the equations mentioned above. The results of the solutions are presented in Table 3. The calculations indicate that after homogenization, the peak homogeneity in a spherical imaging space with a radius of 15 mm is 80.45 ppm. By employing the active homogenization analytical method, the magnetic field in the target area is reduced from 107.41 ppm to 80.45 ppm, thereby enhancing the homogeneity of the magnetic field in the target space.

Additionally, the optimization algorithm provides the required current distribution structure for the uniform field coil, as illustrated in Fig. 6.

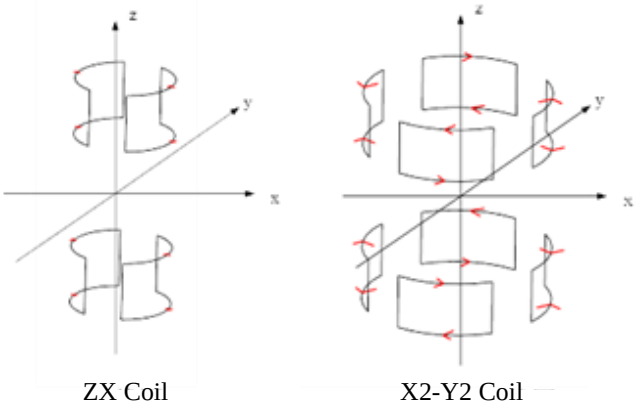

ZX Coil X2-Y2 Coil

Fig. 6 Structure of uniform field coil current

The figure illustrates that the structure of the X coil and the ZX coil is similar, but the direction of the current passing through them is different. Consequently, the formation of the magnetic field structure also differs. Additionally, when assembling the uniform field coils, it is important to follow the order of low-order first and then high-order. In this case, the ZX coil is positioned on the outer side of the X coil. Moreover, the X2-Y2 coils are located outside the ZX coils. Therefore, when applying these coils practically, factors such as the number of turns in each coil, the length of the radius around the cylinder, and the amount of current passing through each turn of the coil must be taken into consideration.

After the above optimization of the uniform field coil, the distribution of the magnetic field on the sphere after uniform field is shown in Fig. 7.

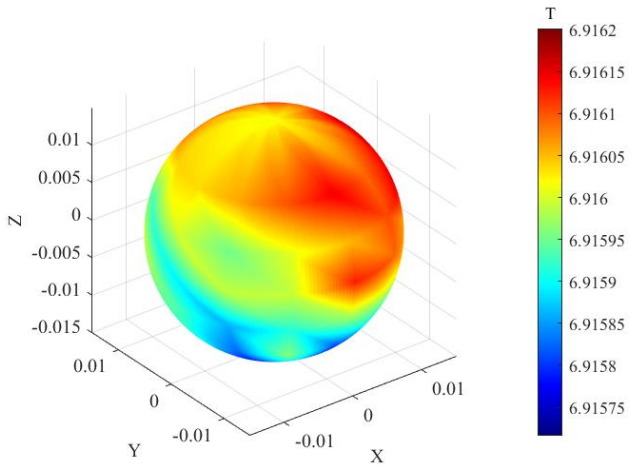

Fig. 7 Visualization of Spherical Magnetic Field after Uniform Field

The harmonic coefficients of each order corresponding to its spherical magnetic field are shown in Table 4

Table 4 Spherical Harmonic Coefficients after Homogenization

A_1^0	A_1^1	B_1^1	$A_2^0/2$	$3gA_2^1$	$3gB_2^1$	$3gA_2^2$	$6gB_2^2$
0.0112	0.0045	0.0017	-0.0654	0.2696	-0.0847	-0.0098	0.0645

The harmonic coefficients were compared before and after homogenization, using the difference in absolute values, as shown in Table 5.

Table 5 Comparison of spherical harmonic coefficients before and after homogenization

Harmonics of all orders	Traditional values	Optimized values	Difference in absolute value
A_1^0	0.025	0.0112	0.0138
A_1^1	0.010	0.0045	0.0055
B_1^1	-0.002	0.0017	0.0003
$A_2^0/2$	-0.371	-0.0654	0.3056
$3gA_2^1$	-0.022	0.2696	-0.2476
$3gB_2^1$	-0.078	-0.0847	-0.0067
$3gA_2^2$	0.010	-0.0098	0.0002
$6gB_2^2$	0.130	0.0645	0.0655

According to the table comparison, it can be concluded that the overall optimization is satisfactory after homogenization. The calculations indicate that after homogenization, the peak uniformity in the spherical imaging space with a radius of 15 mm is 80.45 ppm. By employing the analytical method of active homogenization, the magnetic field in the target area is reduced from 107.41 ppm to 80.45 ppm, thereby enhancing the uniformity of the magnetic field in the target space.

Conclusion

This paper presents a study on the uniform field design of a 7.0T liquid-helium-free magnetic resonance superconducting magnet using the analytical method of quantum genetic optimization and analysis. The main harmonics are decomposed using harmonic analysis, and the active uniform field design is employed to counterbalance the harmonics of each order. The optimization process successfully achieves uniformity in the field of the 7.0T liquid-helium-free magnetic resonance superconducting magnet. Based on the findings, the following conclusions are drawn.

The distribution characteristics of the strong magnetic field generated by the magnetic resonance superconducting magnet were analyzed. Harmonic analysis was conducted to examine the magnetic field in the target region, resulting in a two-dimensional magnetic field distribution map with 8th order harmonics. The structure of the radial uniform field coil was optimized, and the equilibrium relationship between the current and the number of turns was solved using a quantum genetic algorithm. Additionally, an analytical method model was used to establish the axial uniform field coil. It was observed that the magnetic field structure varies significantly when different directions of current are passed through.

In practical coil applications, the number of turns of each coil, the length of the radius of the cylinder, and the magnitude of current passing through each turn of the coil should be taken into consideration. After optimizing the uniform field, the peak uniformity in the spherical imaging space with a radius of 15mm was measured to be 80.45ppm. By employing the analytical method of active uniform field, the magnetic field in the target area was reduced from 107.41ppm to 80.45ppm, resulting in improved uniformity of the magnetic field in the target space. This provides a favorable environment for achieving passive uniform field uniformity subsequently.

Reference

[1]. C.M. Huang, S.S. Chen, J.Q. Zhang et al. Design method of magnetic resonance active uniform-field coils based on target field point method and stream function[J]. Physics Letters, 2019, 68(19):268-274.
[2]. Chu, Y.-S. Active homogenization of MRI magnets [J]. Journal of Electro technology, 1996(05):40-44.
[3]. Wang, Y., Wang, Q., Wang, H., Wang, L., Zhai, Y., Qu, H., Liu, Y., & Liu, F. (2020). Actively-Shielded Superconducting Magnet Design of a Large-Bore 7 T Animal MRI Scanner. IEEE Transactions on Applied Superconductivity, 30(4), 1-4.
[4]. Yue, Z., Sun, Z., & Liu, Z. (2019). Design and Magnetic Field Simulation of 3.0T MRI Superconducting Magnet. IEEE Transactions on Applied Superconductivity, 29(2), 1-6.
[5]. Liang, Z. (2019). An Optimal Design of Actively Shielded MRI Superconducting Magnet. IEEE Transactions on Applied Superconductivity, 29(2), 1-4.
[6]. Iwata, Y., Shirai, T., & Noda, K. (2016). Design of Superconducting Magnets for a Compact Carbon Gantry. IEEE Transactions on Applied Superconductivity
[7]. Thekkethil, S. R., Kar, S., Kumar, M., Soni, V., Suman, N. K., Sharma, R. G., Rastogi, V., & Datta, T. S. (2018). Stress-Induced Magnetic Field Inhomogeneity in a 1.5 T Superconducting MRI Magnet. IEEE Transactions on Applied Superconductivity, 28(4), 1-5.
[8]. Winkler, S. A., Schmitt, F., Landes, H., de Bever, J., Wade, T., Alejski, A., & Rutt, B. K. (2018). 031-Gradient and shim technologies for ultra high field MRI. Neuroimage, 168, 59-70.
[9]. Fayad Z A, Valentin F, Konstantin N, et al. Computed tomography and magnetic resonance imaging for noninvasive coronary angiography and plaque imaging: current and potential future concepts[J]. Circulation, 2002, 106(15): 2026-2034.
[10]. Shandra B, Glas A S, Jacobus V D V, et al. Computed tomography and magnetic resonance imaging in staging of uterine cervical carcinoma: a systematic review [J]. Gynecologic Oncology, 2003, 91(1): 59-66.
[11]. Turner R. A target field approach to optimal coil design [J]. Journal of Physics D Applied Physics, 1986, 19(8): L147-L151.
[12]. Carlson J, Derby K, Hawryszko C, et al. Design and Evaluation of Optimized Shielded Gradient Coils For MRI[C]. 1990 IEEE Nuclear Science Symposium Conference Record, 1990: 1386-1390.
[13]. Petropoulos L S, Morich M A. Novel gradient coil set with an interstitial gap for interventional nuclear magnetic resonance applications [J]. Magnetics IEEE Transactions on Magnetics, 1997, 33(5): 4107-4109.
[14]. Petropoulos L S, Morich M A. Novel gradient coil set with canceled net thrust force for nuclear magnetic resonance applications [J]. IEEE Transactions on Magnetics, 1995, 31(6): 3536-3538.
[15]. Crozier S, Dodd S, Doddrell D M. Design of shielded quadrupolar gradient coils for magnetic resonance microscopy by simulated annealing [J]. IEEE Transactions on Magnetics 1994, 30(3): 1242-1246.
[16]. Siebold H. Gradient field coils for MR imaging with high spectral purity [J]. IEEE Transactions on Magnetics, 1990, 26(2): 897-900.
[17]. Du X, Zhu Z, Zhao L, et al. Design of Cylindrical Transverse Gradient Coil for 1.5 T MRI System[J]. IEEE Transactions on Applied Superconductivity, 2012, 22(3): 1-4.
[18]. Zhu M, Xia L, Liu F, et al. Deformation-Space Method for the Design of Biplanar Transverse Gradient Coils in Open MRI Systems[J]. IEEE Transactions on Magnetics, 2008, 44(8): 2035-2041.
[19]. Zhang P, Shi Y, Wang W, et al. A spiral, bi-planar gradient coil design for open magnetic resonance imaging [J]. Technology and Health Care, 2018, (Preprint): 1-14.
[20]. Wang Y, Xin X, Liu F, et al. Spiral Gradient Coil Design for Use in Cylindrical MRI Systems[J]. IEEE Transactions on Biomedical Engineering 2018, 65(4): 911-920.
[21]. Hidalgo-Tobon S S. Theory of gradient coil design methods for magnetic resonance imaging [J]. Concepts in Magnetic Resonance Part A, 2010, 36(4): 223-242.
[22]. You X F, Yang W H, Song T, et al. Asymmetric Gradient Coil Design by Numerical Approach for MRI Brain Imaging[J]. IEEE Transactions on Applied Superconductivity, 2012, 22(3): 1-5.